Unraveling Metal/Pincer Ligand Effects in the Catalytic Hydrogenation of Carbon Dioxide to Formate

Boodsarin Sawatlon,[a] Matthew D. Wodrich,[a] and Clémence Corminboeuf[a,b]*

[a]Laboratory for Computational Molecular Design, Institute of Chemical Sciences and Engineering, Ecole Polytechnique Fédérale de Lausanne, 1015 Lausanne, Switzerland

[b]National Centre for Computational Design and Discovery of Novel Materials (MARVEL), Ecole Polytechnique Fédérale de Lausanne, 1015 Lausanne, Switzerland

Email: clemence.corminboeuf@epfl.ch

ABSTRACT

The hydrogenation of carbon dioxide to formate is an intriguing reaction from both environmental and energy perspective, primarily due to the prospective uses of the product as a platform chemical in numerous applications such as an organic hydrogen-carrier. While several transition metal based catalysts have been shown to facilitate this chemical transformation, few guidelines exist on how best to tune the catalysts in order to achieve maximum activity. Here, we use linear scaling relationships and molecular volcano plots to gauge the potential of different metal-pincer catalysts for the aforementioned reaction. Analysis of combinations of five metals (Ru, Os, Co, Rh, and Ir) and seven tridentate pincer-type ligands reveal several complexes lying near the volcano top, suggesting that these species have nearly ideal energetic profiles for facilitating the hydrogenation reaction. In particular, catalysts bearing group 9 metal centers (Ir, Rh, Co) with π-acidic ligands provide a clear route to improving catalytic activity. Overall, these findings highlight how linear scaling relationships and molecular volcano plots provide unique insight into the underlying stereoelectronic factors that make specific metal-ligand combinations highly efficient catalysts.

INTRODUCTION

C1 compounds, *e.g.*, methanol, methane, and formic acid/formate salt,[1-7] are important platform chemicals that find use in applications ranging from fabric dyeing and printing processes to hydrogen storage.[8-11] As an example, the hydrogenation of carbon dioxide (CO_2) to formic acid/formate salt provides a promising route using a readily available carbon feedstock[12] to develop liquid organic hydrogen-carriers (LOHCs) systems.[13] The principal shortcoming of the hydrogenation reaction (Figure 1a), however, is that CO_2 is an inherently inert and stable gas, meaning that transition metal catalysts are generally required to facilitate chemical transformations. Such catalytic processes typically operate under

harsh conditions (high temperature and/or pressure of CO_2 and H_2), thus it is hardly surprising that new systems that operate under milder conditions are continuously being developed.[14-17]

To date, the most promising homogeneous hydrogenation pincer-catalysts consist of transition metal complexes (*e.g.,* Ir, Rh, Ru, and Fe) incorporating PNP pincer ligands based on a 2,6-dimethylpyridine scaffold where the P and N atoms are directly bound to the metal center.[18-21] The connecting atoms of the pincer backbone can be swapped with either N and C, which leads to a host of different ligand families (*e.g.*, PNN, NNN, PCP),[22-24] as illustrated in Figure 1b. Perhaps the most well-known homogeneous catalytic system for the hydrogenation of CO_2 to formate used a Ir^{III}-PNP catalyst (PNP=2,6-bis(di-iso-propylphosphinomethyl)pyridine) and yielded a maximum turnover number of 3,500,000.[25-26] Subsequent experimental[27-32] and theoretical[33-41] investigations have also revealed that this, as well as other metal-pincer complexes should be capable of catalyzing the hydrogenation reaction. Nevertheless, despite considerable experimental and computational work, a comprehensive picture on why certain metal/ligand combinations are superior to others remains lacking.

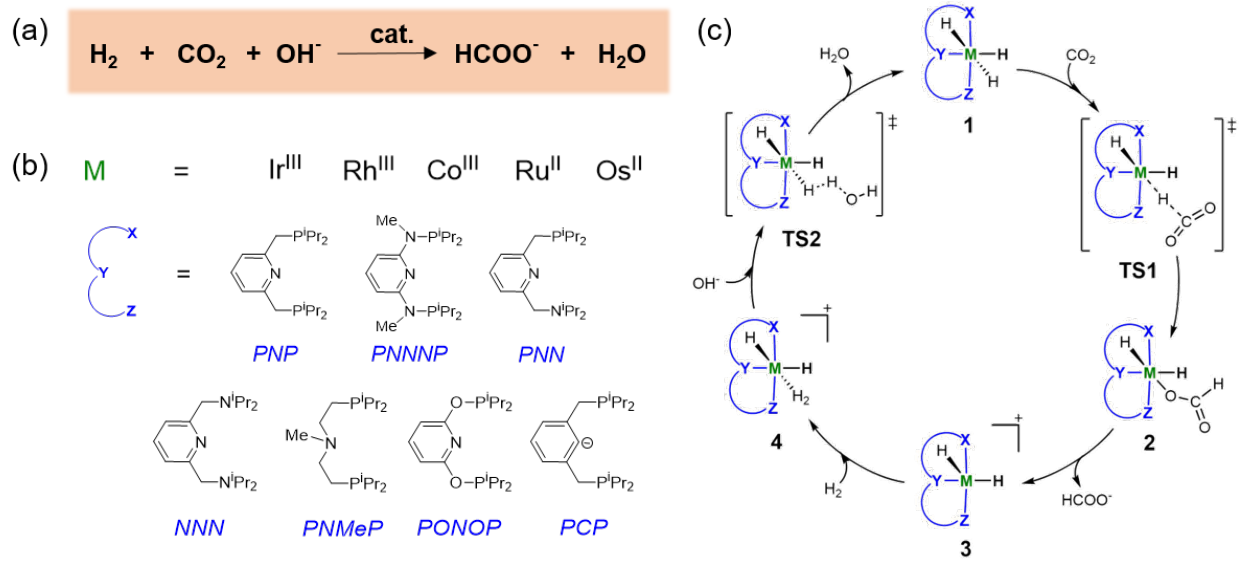

Figure 1. (a) The hydrogenation reaction of carbon dioxide to formate, (b) different metal-ligand combinations studied in this work, and (c) the proposed catalytic cycle.

The first step in uncovering such information is to firmly establish the details of the reaction mechanism, which can provide important evidence on how a catalyst might be modified to improve its activity. For example, the prototypical Ir^{III}-PNP catalyzed hydrogenation of CO_2 (Figure 1c),[37] proceeds through a catalytic cycle that first involves complexation of carbon dioxide with the hydrido (H^-) ligand of **1**, hydride extraction (**TS1**) then ultimately leads to a formate ion bound to the catalyst *via* its oxygen atom, **2**. Dissociation of the formate ion then produces cationic species, **3**, which is followed by the addition of molecular hydrogen (H_2) to form **4**. The heterolytic cleavage of H_2 and abstraction of the proton by a hydroxide base (^-OH) (**TS2**) closes the catalytic cycle by producing a molecule of water and regenerating **1**. Previous computational results have identified the rate-determining step for the Ir^{III}-PNP catalyst as involving heterolytic H_2 cleavage and proton transfer to the hydroxide anion (*i.e.*, **4**→**TS2**).[37] Nonetheless, the kinetic profiles that govern catalytic efficiency, or even the specific rate-determining step itself, may be different for other species. Obtaining this critically important information, however, requires computing the entire catalytic cycle for each individual catalyst, an arduous task that is both time consuming and computationally expensive.

Fortunately, we have recently shown that the kinetic profiles of catalysts can be estimated at greatly reduced computational cost using molecular volcano plots.[42-48] Volcano plots,[49-50] which are widely used in heterogeneous and electrocatalysis,[51-53] and, more recently, have been invoked to rationalize[54-57] and predict[42-48] the performance of homogeneous catalysts. By computing a single descriptor variable for each catalyst, such as the reaction energy of one step of the catalytic cycle, it is possible to assess the thermodynamics or kinetics of the entire catalytic cycle through linear free energy scaling relationships (LFESRs).[58-60] After constructing the volcano plot from the corresponding LFESRs, the properties of various catalysts can be quickly assessed from their position on the plot. Catalysts lying on the plateau or near the peak are considered good candidates that possess balanced substrate/catalyst interactions, in accordance with Sabatier's principle.[61] On the other hand, catalysts located far from the

peak (or plateau) on the left or right slopes have interaction energies that are either too strong (making release of the final products problematic) or too weak (making entry into the catalytic cycle difficult), respectively. Despite being based on thermodynamic concepts, these same principles are valid for kinetic quantities such as transition state barrier heights.[43, 48, 62-66] The objective of this work is to unravel how various metals and ligands work in tandem to catalyze the hydrogenation of carbon dioxide to formate using molecular volcano plots. Using these tools, we reveal guiding principles that deliver strategies for improving the activity of prospective catalysts through manipulation of the catalytic cycle kinetics.

COMPUTATIONAL DETAILS

The geometries of all species were first optimized at the M06[67-68]/def2-SVPD[69] level using the 'ultrafine' integration grid[70] along with the SMD[71] implicit solvation model (solvent=water) in Gaussian09.[72] An analysis of the resulting vibrational frequencies ensured that each structure was either a minima (zero imaginary frequencies) or a transition state (one imaginary frequency) on the potential energy surface. To obtain a complementary picture of the catalyst free energies profiles, single point electronic energies were determined on the M06 optimized geometries using the B3LYP[73-74] functional appended with a density-dependent dispersion correction –dDsC[75-78] (*i.e.*, B3LYP-dDsC) in tandem with the aug-TZ2P (TZ2P for the transition metal species) Slater-type basis sets as implemented in ADF.[79-80] Free energy corrections (at 298K and 1 atm from the M06 computations) were determined using the rigid-rotor harmonic oscillator model (as proposed by Grimme[81]) along with a correction for translational entropy in solution (as proposed by Whitesides[82]) within the GoodVibes program[83] developed by Paton and Funes-Ardoiz. Final solvation correction values (in water) were then determined at the B3LYP-dDsC/aug-TZ2P level using the COSMO-RS solvation model,[84] also as implemented in ADF. For all intermediates and transition states, wave function stability was tested to confirm that the singlet state is the ground state.

RESULTS AND DISCUSSION

Linear free energy scaling relationships. Based on the reaction mechanism depicted in Figure 1c, we computed free energies for each of the catalytic cycle intermediates and transition states for a total of 35 pincer catalysts (combinations of five metals and seven ligands shown in Figure 1b). Analysis of the Figure 1c reaction mechanism, as well as an alternative ligand cooperative pathway (see SI for details), confirmed the favorability of the non-cooperative mechanism.[25, 37-38] Linear free energy scaling relationships (LFESRs) were then established by calculating the stabilities of each intermediate and transition state **r**elative to a **r**eference **s**tate (ΔG_{RRS}), which we selected as the entry point into the catalytic cycle, **1**. An assessment of different potential descriptor variables identified ΔG_{RRS}(**4**) (as defined in Eq. 1) as being the most suitable, as strong LFESRs exist between this variable and the stabilities of other catalytic cycle intermediates and transitions states, as illustrated in Figure 2.

$$\mathbf{1} + CO_2 + H_2 \rightarrow \mathbf{4} + HCOO^- \qquad \Delta G_{RRS}(\mathbf{4}) \qquad \text{Eq. 1}$$

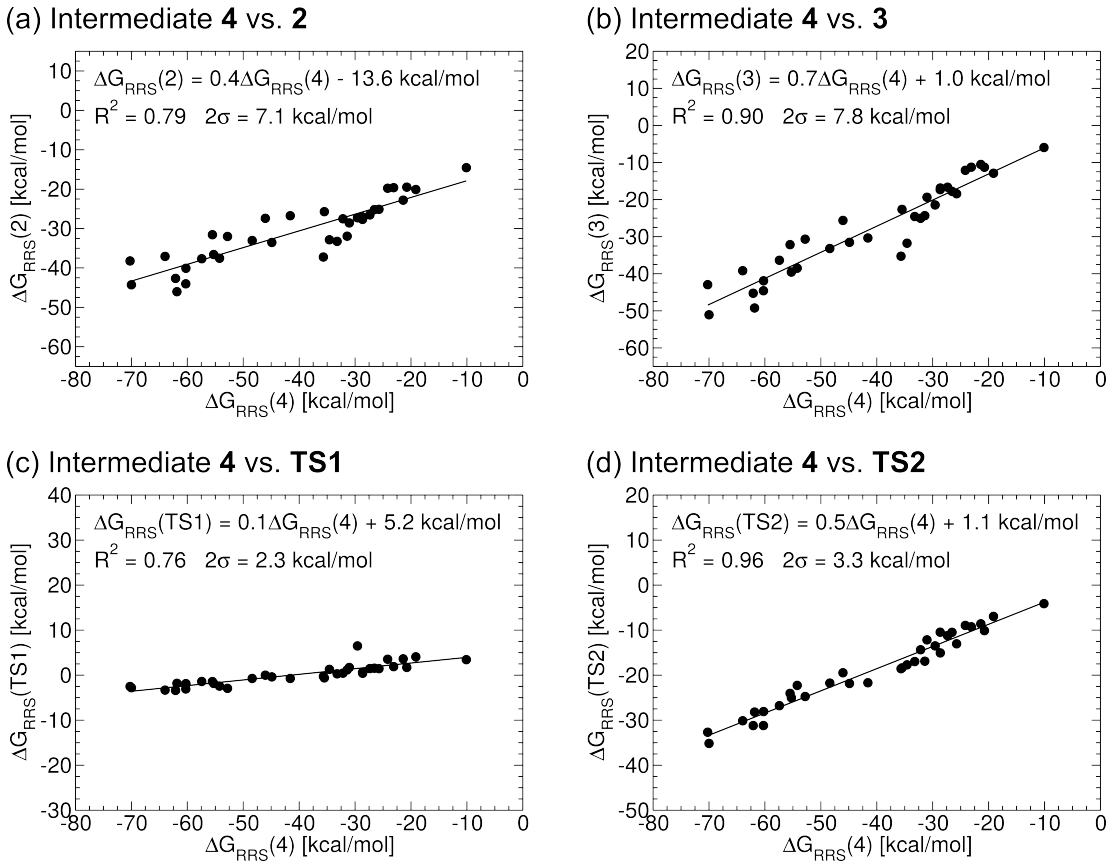

Figure 2. Linear free energy scaling relationships between the descriptor variable, ΔG_{RRS}(**4**) and intermediates [ΔG_{RRS}(**2**) (a) and ΔG_{RRS}(**3**) (b)] as well as transition states [ΔG_{RRS}(**TS1**) (c) and ΔG_{RRS}(**TS2**) (d)] for the hydrogenation of carbon dioxide to formate. All free energies (ΔG_{RRS}) are relative to the reference state (RRS), **1**. Knowing the value of the descriptor, ΔG_{RRS}(**4**), (plotted on the x-axis) allows the prediction of the relative stability of other intermediates and transition states present in the catalytic cycle directly from these scaling relationships.

Molecular volcano plots. Having established LFESRs along with a suitable descriptor variable, the Figure 1 reaction can be cast into a simulated reaction profile (Figure 3a). This profile provides an estimate of the free energy associated with moving between any two linked intermediates and transition states of the catalytic cycle directly by knowing the value of the descriptor [*e.g.,* ΔG_{RRS}(**4**)] for the reaction. The overall nature of the steps largely agrees with previous work. For instance, formation of the formate ion through hydride abstraction from the catalyst by CO_2 is shown to be a very energetically

facile process (*i.e.*, the black line indicates most values are roughly thermoneutral), in agreement with the recent work of Heimann *et al*.[85] Moreover, in many cases proton abstraction by the hydroxide basis in anticipated to be the rate determining step (*i.e.*, the magenta line predicts very endergonic reaction values for species falling in the left section of the plot), as is the case for the aforementioned Ir^{III}-PNP catalyst.[37]

The final volcano plot (Figure 3b) can be obtained directly from the simulated reaction profile (Figure 3a) by taking only the most energetically costly reaction step [*i.e.*, the **k**inetic **d**etermining **s**tep, -ΔG(kds), plotted along the y-axis] for each descriptor (x-axis) value. For the hydrogenation of CO_2 to formate, the volcano plot is divided into two sections, each of which is governed by a different reaction step that is the most energetically costly. The two steps correspond to the dissociation of the oxygen bound formate ion from the catalyst (**2→3**) as well as heterolytic H_2 cleavage and proton abstraction by the hydroxide base (**4→TS2**). Curiously, in contrast to the more typically seen molecular volcano picture in which the slopes can be directly interpreted as paralleling substrate binding (*i.e.*, oxidative addition) and product release (*i.e.*, reductive elimination), the Figure 3 plot is a bit more complicated. While our previous work used the binding energy of a substrate directly with the metal center as a descriptor variable,[42-46, 48] here the chosen descriptor represents the energy difference between the binding of a hydrido ligand (**1**) and molecular H_2 (**4**). As such, the typical strong-binding/weak-binding nature of the left/right slopes becomes harder to distinguish, yet remains present. In essence, species with negative x-axis values have stronger interaction with molecular hydrogen than with a hydride ion. Thus, catalysts falling on the left slope bind H_2 in an overly strong fashion, making the transition from H_2 to H^- (*i.e.*, **4→TS2**) difficult and energetically costly. Moving rightward along the x-axis, species will have an increasingly strong interaction for H^- and an accompanying reduction in H_2 binding ability, which manifests itself in a gradual reduction in the **4→TS2** barrier height. Ultimately, the ability of the catalysts to bind anionic species (such as H^- or formate ion) becomes quite strong, which causes the release of oxygen bound formate species (**2→3**) to become the most energetically costly reaction step.[86] Taken as a

whole, the Figure 3b volcano plot indicates that an ideal hydrogenation catalyst must have a finely tuned ability to bind both neutral (*e.g.*, molecular hydrogen) and anionic (*e.g.*, hydride and formate), each of which are present in the catalytic cycle, neither too weakly nor too strongly.

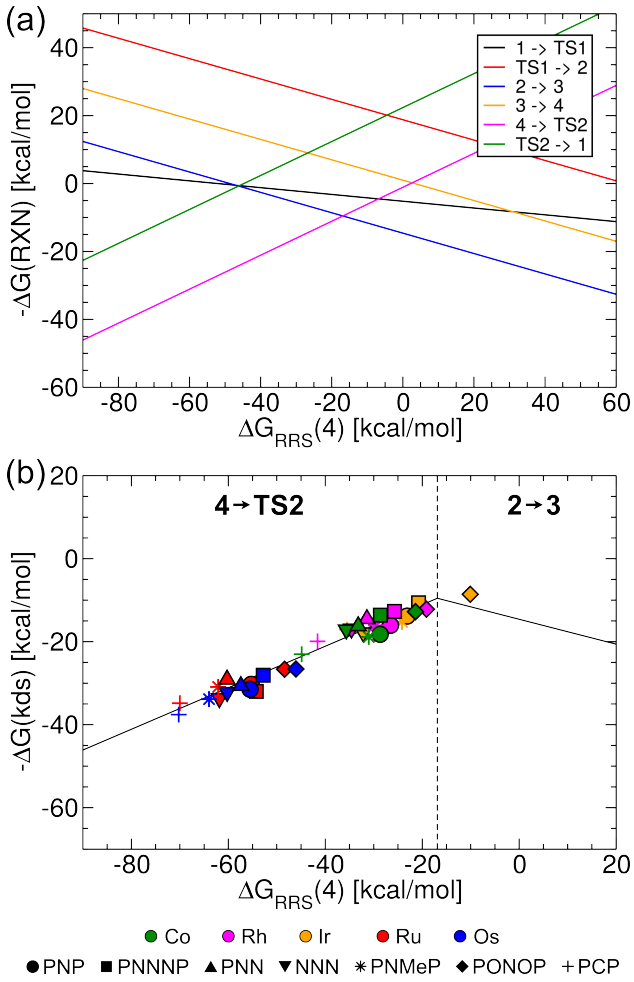

Figure 3. (a) Simulated reaction profile depicting the anticipated energy associated with each step [ΔG(RXN)] of the catalytic cycle for a specific value of the descriptor variable (x-axis). (b) A volcano plot that illustrates anticipated activity for the hydrogenation of CO_2 to formate by predicting the value of the most energetically difficult reaction step to complete [*e.g.*, the kinetic determining step (kds)]. The volcano plot is split into two sections by the vertical dashed line, which indicates a change in the nature of the most difficult reaction step of the catalytic cycle. Note that Ir(PNP) (orange circle) is an experimentally known catalyst that facilitates the hydrogenation reaction.

Individual catalysts are placed onto the volcano according to their energy-based descriptor (x-axis) and the free energy associated with the appropriate kinetic determining step (kds, y-axis). For the 35 catalysts tested here, a vast majority fall on the left side of the volcano, meaning that the most energetically costly reaction step is the heterolytic H_2 cleavage and proton transfer (**4→TS2**). As mentioned earlier, this matches the findings of a previous computational study of Ir(PNP) pincer.[37] The sole exception is Ir(PONOP) (orange diamond, Figure 3), which lies on the opposing side of the volcano as the other catalysts where the most costly step is dissociation of the formate ion (**2→3**).

A closer examination of Figure 3b shows that the catalysts are roughly grouped into two regions based on their metal center. Catalysts bearing group 9 metals (Co, Rh, Ir) lie closer to the volcano peak, indicating that they are anticipated to more pronounced ability to catalyze the reaction in question than group 8 metals (Ru, Os), which fall further from the volcano peak along the strong-binding (left) slope. As expected, the experimentally characterized Ir(PNP) complex[25] (orange circle, Figure 3b) is amongst a handful of catalysts that the volcano plot predicts will have nearly maximal activity. Other species having roughly comparable activities to Ir(PNP) include: Ir(PONOP), Rh(PONOP), and Co(PONOP). The later should be of particular interest given the cost associated with using earth-abundant metals to catalyze reactions. On the other hand, the Ru and Os catalysts studied here show significant stabilization of the catalytic cycle intermediates,[87] particularly **4**, relative to the desired reaction product (see SI Table S1) and are far from the volcano peak. As such, these species are anticipated to exhibit minimal activity for the hydrogenation of CO_2.

Figure 4 provides a free energy diagram that depicts the catalytic energetics for these four species. As expected, the highest energy barriers of these species are identical to those predicted by the volcano plot, indicating that the free energy predictions made by the linear free energy scaling relationships closely match actual values obtained directly from DFT computations. For Ir(PNP), Rh(PONOP), and Co(PONOP), heterolytic H_2 cleavage and proton transfer (**4→TS2**) is most costly and

requires 13.8, 12.2, and 12.8 kcal/mol, respectively. In contrast, Ir(PONOP) needs only 6.0 kcal/mol to complete this reaction step. For Ir(PONOP), the most costly reaction step is dissociation of the formate ion (**2→3**), which requires 8.6 kcal/mol. Overall, Figure 4 shows that all of these catalysts experimentally viable, with Ir(PONOP) anticipated to have particularly good activity.

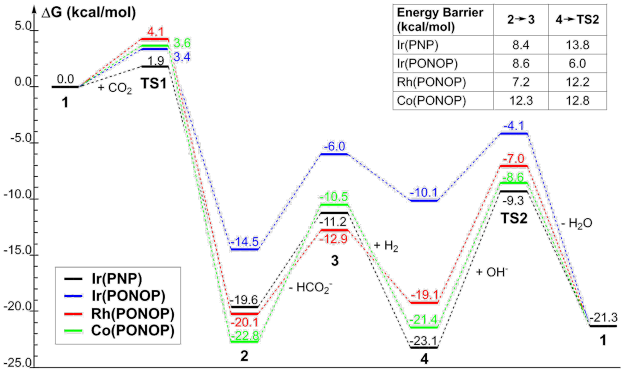

Figure 4. Computed free energy diagrams of the catalytic cycles of selected species.

Despite the fact that all catalysts appear to be clustered according to their metal center, the nature of the ligand does have an influence on the efficiency of the catalytic process. These changes become most evident if the relative positions of ligands are considered. Clear trends emerge if we arbitrarily set the PNP-ligand complexes for each metal type as the "zero point" and plot the corresponding shifts to weaker or stronger binding of the other ligands. This reveals, for instance, that the PONOP ligand produces a considerable shift of a catalyst toward weaker binding (*i.e.*, right along the x-axis, Figure 5). Since the Rh(PNP) and Co(PNP) catalysts already lie on the strong binding (left) side of the volcano peak, the rightward shift brought about by replacing the PNP with the PONOP ligand leads to enhanced activity, as indicated by Rh(PONOP) and Ir(PONOP) being closer to the volcano peak than Rh(PNP) and Ir(PNP). A smaller, yet similar effect is seen for the PNNNP ligand (Figure 5). In contrast, the PCP ligand provides an opposing effect, producing a significant shift toward stronger binding (*i.e.*, leftward along the x-axis, Figure 5). For the reaction studied here, replacing the PNP ligand with a PCP ligand reduces catalytic activity by shifting all catalyst leftward away from the volcano peak (Figure 3b). The use of

NNN, PNMeP and PNN ligands also produce similar, yet less dramatic, leftward shifts along the volcano plot.

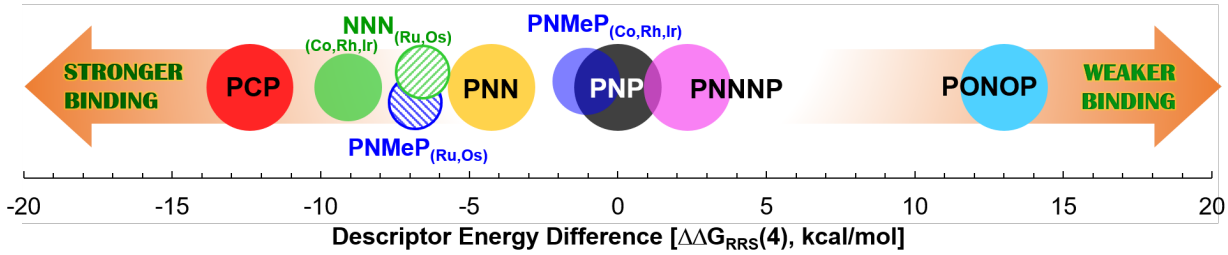

Figure 5. The average deviation of different pincer ligands on the volcano plots from the PNP ligand, which is used as a reference and arbitrarily set to zero. The influence of the ligand on the descriptor value ([ΔG_{RRS}(**4**)], *i.e.,* the x-axis in the Figure 3b volcano plot) is then measured by subtracting each ligand value with the PNP complex of the same metal. Different colored dots indicate the influence of different ligands. For example, the PONOP ligand causes of a shift of ~13 kcal/mol to the right of the volcano plot relative to the PNP ligand (*e.g.*, in the Figure 3b volcano plot, the descriptor value for Ir(PNP) is -23.10 kcal/mol and Ir(PONOP) is -10.10 kcal/mol).

Further in depth examination also uncovers the influence of the pincer ligand's connecting atoms (X, Y, and Z symbols in Figure 1). In essence, when the flanking X and Z atoms (*i.e.*, as in the PNP, PNN, and NNN ligands), as well as the central pincer atom (Y = $N_{pyridine}$, N_{amine}, and C_{phenyl} in PNP, PNMeP, and PCP respectively), are strong π-acceptor/more π-acidic moieties, such as phosphorus, the position of the catalyst tend to fall further to the right on the volcano plot than other pincer ligands with the same metal type (Figure 5), indicative of a weaker catalyst/substrate binding interaction.[88-89] Collectively, these 'ligand backbone effects' are known to significantly impact overall catalytic performance.[90] Moreover, changing the number or type of connecting atoms located between the X and Y or the Y and Z atoms also influences activity, as is clearly evident by examining difference between the PONOP, PNNNP, and PNP complexes. The presence of more electronegative oxygen atoms in the PONOP-ligand produces a larger shift of the catalysts toward weak binding (rightward along the x-axis) than the less electronegative N and C atoms found in PNNNP and PNP. As such, the clearest path toward improving catalytic performance is utilizing π-acidic ligands with group 9 metals (Ir, Rh, Co). Doing so

will reduce the energy associated with heterolytic H_2 cleavage and proton transfer that represents the most energetically costly step of the catalytic cycle.

CONCLUSIONS

In conclusion, an examination of the hydrogenation of CO_2 to formate using molecular volcano plots shows that myriad metal and pincer ligand combinations have the ability to catalyze this reaction. Of a set of 35 catalysts tested, iridium, rhodium and cobalt complexes with π-acidic ligands stand out as having particularly attractive catalytic cycle energetic profiles. For nearly all of the tested catalysts, the heterolytic H_2 cleavage and the proton transfer to hydroxide base represent the most energetically costly step of the catalytic cycle. This energetic cost, however, can be minimized and the overall kinetics of the reaction improved by selecting catalysts bearing a strong π-accepting pincer ligand. Overall, this work demonstrates how molecular volcano plots can be used not only for estimating the performance of and designing new catalytic species, but also for uncovering the underlying trends that make functional catalysts tick.

Supporting Information

Supporting information is available free of charge on the ACS Publications website at DOI:

Details of volcano construction, free energies for the catalytic cycle of each species, and computed electronic energies, enthalpies, and free energies (pdf)

Cartesian coordinates of all computed structures (zip)

AUTHOR INFORMATION

Corresponding Author

*E-mail: clemence.corminboeuf@epfl.ch

ORCID

Boodsarin Sawatlon: 0000-0002-1600-022X

Matthew D. Wodrich: 0000-0002-6006-671X

Clémence Corminboeuf: 0000-0001-7993-2879

ACKNOWLEDGMENTS

The EPFL and the Swiss National Science Foundation (Grant No. 200020_175496) are acknowledged for financial support.

REFERENCES

1. Álvarez, A.; Bansode, A.; Urakawa, A.; Bavykina, A. V.; Wezendonk, T. A.; Makkee, M.; Gascon, J.; Kapteijn, F., Challenges in the Greener Production of Formates/Formic Acid, Methanol, and DME by Heterogeneously Catalyzed CO_2 Hydrogenation Processes. *Chem. Rev.* **2017,** *117*, 9804-9838.

2. Gunasekar, G. H.; Park, K.; Jung, K.-D.; Yoon, S., Recent Developments in the Catalytic Hydrogenation of CO_2 to Formic Acid/Formate using Heterogeneous Catalysts. *Inorg. Chem. Front.* **2016,** *3*, 882-895.

3. Upadhyay, P.; Srivastava, V., Carbon Sequestration: Hydrogenation of CO_2 to Formic Acid. In *Present Environment and Sustainable Development*, 2016; Vol. 10, p 13.

4. Ashley, A. E.; Thompson, A. L.; O'Hare, D., Non-Metal-Mediated Homogeneous Hydrogenation of CO_2 to CH_3OH. *Angew. Chem. Int. Ed.* **2009,** *48*, 9839-9843.

5. Ménard, G.; Stephan, D. W., Room Temperature Reduction of CO_2 to Methanol by Al-Based Frustrated Lewis Pairs and Ammonia Borane. *J. Am. Chem. Soc.* **2010,** *132*, 1796-1797.

6. Berkefeld, A.; Piers, W. E.; Parvez, M., Tandem Frustrated Lewis Pair/Tris(pentafluorophenyl)borane-Catalyzed Deoxygenative Hydrosilylation of Carbon Dioxide. *J. Am. Chem. Soc.* **2010,** *132*, 10660-10661.

7. Wang, W.-H.; Himeda, Y.; Muckerman, J. T.; Manbeck, G. F.; Fujita, E., CO_2 Hydrogenation to Formate and Methanol as an Alternative to Photo- and Electrochemical CO_2 Reduction. *Chem. Rev.* **2015,** *115*, 12936-12973.

8. Johnson, W., Jr. ; Heldreth, B.; Bergfeld, W. F.; Belsito, D. V.; Hill, R. A.; Klaassen, C. D.; Liebler, D. C.; Marks, J. G., Jr.; Shank, R. C.; Slaga, T. J.; Snyder, P. W.; Andersen, F. A., Safety Assessment of Formic Acid and Sodium Formate as Used in Cosmetics. *Int. J. Toxicol.* **2016,** *35*, 41S-54S.

9. He, T.; Pachfule, P.; Wu, H.; Xu, Q.; Chen, P., Hydrogen Carriers. *Nat. Rev. Mater.* **2016,** *1*, 16059.

10. Zhong, H.; Iguchi, M.; Chatterjee, M.; Himeda, Y.; Xu, Q.; Kawanami, H., Formic Acid-Based Liquid Organic Hydrogen Carrier System with Heterogeneous Catalysts. *Adv. Sustainable Syst.* **2018,** *2*, 1700161.

11. Formic Acid. In *Ullmann's Encyclopedia of Industrial Chemistry*.

12. Sakakura, T.; Choi, J.-C.; Yasuda, H., Transformation of Carbon Dioxide. *Chem. Rev.* **2007,** *107*, 2365-2387.

13. Sordakis, K.; Tang, C.; Vogt, L. K.; Junge, H.; Dyson, P. J.; Beller, M.; Laurenczy, G., Homogeneous Catalysis for Sustainable Hydrogen Storage in Formic Acid and Alcohols. *Chem. Rev.* **2018,** *118*, 372-433.

14. Ohnishi, Y.-y.; Nakao, Y.; Sato, H.; Sakaki, S., Ruthenium(II)-Catalyzed Hydrogenation of Carbon Dioxide to Formic Acid. Theoretical Study of Significant Acceleration by Water Molecules. *Organometallics* **2006,** *25*, 3352-3363.

15. Rohmann, K.; Kothe, J.; Haenel, M. W.; Englert, U.; Hölscher, M.; Leitner, W., Hydrogenation of $CO_{(2)}$ to Formic Acid with a Highly Active Ruthenium Acriphos Complex in DMSO and DMSO/Water. *Angew. Chem., Int. Ed. Engl.* **2016,** *55*, 8966-8969.

16. Ge, H.; Chen, X.; Yang, X., Hydrogenation of Carbon Dioxide to Methanol Catalyzed by Iron, Cobalt, and Manganese Cyclopentadienone Complexes: Mechanistic Insights and Computational Design. *Chem. Eur. J.* **2017,** *23*, 8850-8856.

17. Schneidewind, J.; Adam, R.; Baumann, W.; Jackstell, R.; Beller, M., Low-Temperature Hydrogenation of Carbon Dioxide to Methanol with a Homogeneous Cobalt Catalyst. *Angew. Chem. Int. Ed.* **2017,** *56*, 1890-1893.

18. Chakraborty, S.; Lagaditis, P. O.; Förster, M.; Bielinski, E. A.; Hazari, N.; Holthausen, M. C.; Jones, W. D.; Schneider, S., Well-Defined Iron Catalysts for the Acceptorless Reversible Dehydrogenation-Hydrogenation of Alcohols and Ketones. *ACS Catal.* **2014,** *4*, 3994-4003.

19. Bernskoetter, W. H.; Hazari, N., Reversible Hydrogenation of Carbon Dioxide to Formic Acid and Methanol: Lewis Acid Enhancement of Base Metal Catalysts. *Acc. Chem. Res.* **2017,** *50*, 1049-1058.

20. Zeng, G.; Maeda, S.; Taketsugu, T.; Sakaki, S., Catalytic Hydrogenation of Carbon Dioxide with Ammonia–Borane by Pincer-Type Phosphorus Compounds: Theoretical Prediction. *J. Am. Chem. Soc.* **2016,** *138*, 13481-13484.

21. Werkmeister, S.; Neumann, J.; Junge, K.; Beller, M., Pincer-Type Complexes for Catalytic (De)Hydrogenation and Transfer (De)Hydrogenation Reactions: Recent Progress. *Chem. Eur. J.* **2015,** *21*, 12226-12250.

22. Arduengo, A. J.; Stewart, C. A.; Davidson, F.; Dixon, D. A.; Becker, J. Y.; Culley, S. A.; Mizen, M. B., The Synthesis, Structure, and Chemistry of 10-Pn-3 Systems: Tricoordinate Hypervalent Pnicogen Compounds. *J. Am. Chem. Soc.* **1987,** *109*, 627-647.

23. Culley, S. A.; Arduengo, A. J., Synthesis and Structure of the First 10-P-3 Species. *J. Am. Chem. Soc.* **1984,** *106*, 1164-1165.

24. Lawrence, M. A. W.; Green, K.-A.; Nelson, P. N.; Lorraine, S. C., Review: Pincer Ligands—Tunable, Versatile and Applicable. *Polyhedron* **2018,** *143*, 11-27.

25. Tanaka, R.; Yamashita, M.; Nozaki, K., Catalytic Hydrogenation of Carbon Dioxide Using Ir(III)−Pincer Complexes. *J. Am. Chem. Soc.* **2009,** *131*, 14168-14169.

26. Osadchuk, I.; Tamm, T.; Ahlquist, M. S. G., Theoretical Investigation of a Parallel Catalytic Cycle in CO_2 Hydrogenation by (PNP)IrH_3. *Organometallics* **2015,** *34*, 4932-4940.

27. Filonenko, G. A.; van Putten, R.; Schulpen, E. N.; Hensen, E. J. M.; Pidko, E. A., Highly Efficient Reversible Hydrogenation of Carbon Dioxide to Formates Using a Ruthenium PNP-Pincer Catalyst. *ChemCatChem* **2014,** *6*, 1526-1530.

28. Filonenko, G. A.; Conley, M. P.; Copéret, C.; Lutz, M.; Hensen, E. J. M.; Pidko, E. A., The Impact of Metal–Ligand Cooperation in Hydrogenation of Carbon Dioxide Catalyzed by Ruthenium PNP Pincer. *ACS Catal.* **2013,** *3*, 2522-2526.

29. Vogt, M.; Gargir, M.; Iron, M. A.; Diskin-Posner, Y.; Ben-David, Y.; Milstein, D., A New Mode of Activation of CO_2 by Metal–Ligand Cooperation with Reversible C-C and M-O Bond Formation at Ambient Temperature. *Chem. Eur. J.* **2012,** *18*, 9194-9197.

30. Schmeier, T. J.; Dobereiner, G. E.; Crabtree, R. H.; Hazari, N., Secondary Coordination Sphere Interactions Facilitate the Insertion Step in an Iridium(III) CO_2 Reduction Catalyst. *J. Am. Chem. Soc.* **2011,** *133*, 9274-9277.

31. Langer, R.; Diskin-Posner, Y.; Leitus, G.; Shimon, L. J. W.; Ben-David, Y.; Milstein, D., Low-Pressure Hydrogenation of Carbon Dioxide Catalyzed by an Iron Pincer Complex Exhibiting Noble Metal Activity. *Angew. Chem. Int. Ed.* **2011,** *50*, 9948-9952.

32. Huff, C. A.; Sanford, M. S., Catalytic CO_2 Hydrogenation to Formate by a Ruthenium Pincer Complex. *ACS Catal.* **2013,** *3*, 2412-2416.

33. Rawat, K. S.; Pathak, B., Aliphatic Mn-PNP Complexes for the CO_2 Hydrogenation Reaction: a Base Free Mechanism. *Catal. Sci. Technol.* **2017,** *7*, 3234-3242.

34. Filonenko, G. A.; Smykowski, D.; Szyja, B. M.; Li, G.; Szczygieł, J.; Hensen, E. J. M.; Pidko, E. A., Catalytic Hydrogenation of CO_2 to Formates by a Lutidine-Derived Ru–CNC Pincer Complex: Theoretical Insight into the Unrealized Potential. *ACS Catal.* **2015,** *5*, 1145-1154.

35. Filonenko, G. A.; Cosimi, E.; Lefort, L.; Conley, M. P.; Copéret, C.; Lutz, M.; Hensen, E. J. M.; Pidko, E. A., Lutidine-Derived Ru-CNC Hydrogenation Pincer Catalysts with Versatile Coordination Properties. *ACS Catal.* **2014,** *4*, 2667-2671.

36. Bernskoetter, W. H.; Hazari, N., A Computational Investigation of the Insertion of Carbon Dioxide into Four- and Five-Coordinate Iridium Hydrides. *Eur. J. Inorg. Chem.* **2013,** *2013*, 4032-4041.

37. Yang, X., Hydrogenation of Carbon Dioxide Catalyzed by PNP Pincer Iridium, Iron, and Cobalt Complexes: A Computational Design of Base Metal Catalysts. *ACS Catal.* **2011,** *1*, 849-854.

38. Ahlquist, M. S. G., Iridium Catalyzed Hydrogenation of CO_2 under Basic Conditions—Mechanistic Insight from Theory. *J. Mol. Catal. A: Chem.* **2010,** *324*, 3-8.

39. Praveen, C. S.; Comas-Vives, A.; Copéret, C.; VandeVondele, J., Role of Water, CO_2, and Noninnocent Ligands in the CO_2 Hydrogenation to Formate by an Ir(III) PNP Pincer Catalyst Evaluated by Static-DFT and ab Initio Molecular Dynamics under Reaction Conditions. *Organometallics* **2017,** *36*, 4908-4919.

40. Tanaka, R.; Yamashita, M.; Chung, L. W.; Morokuma, K.; Nozaki, K., Mechanistic Studies on the Reversible Hydrogenation of Carbon Dioxide Catalyzed by an Ir-PNP Complex. *Organometallics* **2011,** *30*, 6742-6750.

41. Li, J.; Yoshizawa, K., Catalytic Hydrogenation of Carbon Dioxide with a Highly Active Hydride on Ir(III)–Pincer Complex: Mechanism for CO_2 Insertion and Nature of Metal–Hydride Bond. *Bull. Chem. Soc. Jpn.* **2011,** *84*, 1039-1048.

42. Busch, M.; Wodrich, M. D.; Corminboeuf, C., Linear Scaling Relationships and Volcano Plots in Homogeneous Catalysis - Revisiting the Suzuki Reaction. *Chem. Sci.* **2015,** *6*, 6754-6761.

43. Wodrich, M. D.; Busch, M.; Corminboeuf, C., Accessing and Predicting the Kinetic Profiles of Homogeneous Catalysts from Volcano Plots. *Chem. Sci.* **2016,** *7*, 5723-5735.

44. Busch, M.; Wodrich, M. D.; Corminboeuf, C., A Generalized Picture of C–C Cross-Coupling. *ACS Catal.* **2017,** *7*, 5643-5653.

45. Wodrich, M. D.; Sawatlon, B.; Busch, M.; Corminboeuf, C., On the Generality of Molecular Volcano Plots. *ChemCatChem* **2018,** *10*, 1586-1591.

46. Busch, M.; Wodrich, M. D.; Corminboeuf, C., Improving the Thermodynamic Profiles of Prospective Suzuki–Miyaura Cross-Coupling Catalysts by Altering the Electrophilic Coupling Component. *ChemCatChem* **2018,** *10*, 1592-1597.

47. Meyer, B.; Sawatlon, B.; Heinen, S. N.; von Lilienfeld, A.; Corminboeuf, C., Machine Learning Meets Volcano Plots: Computational Discovery of Cross-Coupling Catalysts. *Chem. Sci.* **2018,** *9*, 7069-7077.

48. Wodrich, M. D.; Busch, M.; Corminboeuf, C., Expedited Screening of Active and Regioselective Catalysts for the Hydroformylation Reaction. *Helv. Chim. Acta* **2018,** *101*, e1800107.

49. Parsons, R., The Rate of Electrolytic Hydrogen Evolution and the Heat of Adsorption of Hydrogen. *Trans. Faraday Society* **1958,** *54*, 1053-1063.

50. Gerischer, H., Mechanism of Electrolytic Discharge of Hydrogen and Adsorption Energy of Atomic Hydrogen. *Bull. Soc. Chim. Belg.* **1958,** *67*, 506.

51. Nørskov, J. K.; Bligaard, T.; Rossmeisl, J.; Christensen, C. H., Towards the Computational Design of Solid Catalysts. *Nat. Chem.* **2009,** *1*, 37.

52. Seh, Z. W.; Kibsgaard, J.; Dickens, C. F.; Chorkendorff, I.; Nørskov, J. K.; Jaramillo, T. F., Combining Theory and Experiment in Electrocatalysis: Insights into Materials Design. *Science* **2017,** *355*.

53. Medford, A. J.; Vojvodic, A.; Hummelshøj, J. S.; Voss, J.; Abild-Pedersen, F.; Studt, F.; Bligaard, T.; Nilsson, A.; Nørskov, J. K., From the Sabatier Principle to a Predictive Theory of Transition-Metal Heterogeneous Catalysis. *J. Catal.* **2015,** *328*, 36-42.

54. Kozuch, S.; Shaik, S., A Combined Kinetic−Quantum Mechanical Model for Assessment of Catalytic Cycles: Application to Cross-Coupling and Heck Reactions. *J. Am. Chem. Soc.* **2006,** *128*, 3355-3365.

55. Kozuch, S.; Shaik, S., Kinetic-Quantum Chemical Model for Catalytic Cycles: The Haber−Bosch Process and the Effect of Reagent Concentration. *J. Phys. Chem. A* **2008,** *112*, 6032-6041.

56. Kozuch, S.; Shaik, S., How to Conceptualize Catalytic Cycles? The Energetic Span Model. *Acc. Chem. Res.* **2011,** *44*, 101-110.

57. Swiegers, G., *Mechanical Catalysis: Methods of Enzymatic, Homogeneous, and Heterogeneous Catalysis*. Wiley: 2008.

58. Calle-Vallejo, F.; Martínez, J. I.; García-Lastra, J. M.; Rossmeisl, J.; Koper, M. T. M., Physical and Chemical Nature of the Scaling Relations between Adsorption Energies of Atoms on Metal Surfaces. *Phys. Rev. Lett.* **2012,** *108*, 116103.

59. Man, I. C.; Su, H.-Y.; Calle-Vallejo, F.; Hansen, H. A.; Martínez, J. I.; Inoglu, N. G.; Kitchin, J.; Jaramillo, T. F.; Nørskov, J. K.; Rossmeisl, J., Universality in Oxygen Evolution Electrocatalysis on Oxide Surfaces. *ChemCatChem* **2011,** *3*, 1159-1165.

60. Abild-Pedersen, F.; Greeley, J.; Studt, F.; Rossmeisl, J.; Munter, T. R.; Moses, P. G.; Skúlason, E.; Bligaard, T.; Nørskov, J. K., Scaling Properties of Adsorption Energies for Hydrogen-Containing Molecules on Transition-Metal Surfaces. *Phys. Rev. Lett.* **2007,** *99*, 016105.

61. Sabatier, P., *La Catalyse en Chimie Organique*. Librairie polytechnique: 1913.

62. Zaffran, J.; Michel, C.; Delbecq, F.; Sautet, P., Trade-Off between Accuracy and Universality in Linear Energy Relations for Alcohol Dehydrogenation on Transition Metals. *J. Phys. Chem. C* **2015,** *119*, 12988-12998.

63. Sutton, J. E.; Vlachos, D. G., A Theoretical and Computational Analysis of Linear Free Energy Relations for the Estimation of Activation Energies. *ACS Catal.* **2012,** *2*, 1624-1634.

64. Santen, R. A. v.; Neurock, M.; Shetty, S. G., Reactivity Theory of Transition-Metal Surfaces: A Brønsted−Evans−Polanyi Linear Activation Energy−Free-Energy Analysis. *Chem. Rev.* **2010,** *110*, 2005-2048.

65. Michaelides, A.; Liu, Z. P.; Zhang, C. J.; Alavi, A.; King, D. A.; Hu, P., Identification of General Linear Relationships between Activation Energies and Enthalpy Changes for Dissociation Reactions at Surfaces. *J. Am. Chem. Soc.* **2003,** *125*, 3704-3705.

66. Nørskov, J. K.; Bligaard, T.; Logadottir, A.; Bahn, S.; Hansen, L. B.; Bollinger, M.; Bengaard, H.; Hammer, B.; Sljivancanin, Z.; Mavrikakis, M.; Xu, Y.; Dahl, S.; Jacobsen, C. J. H., Universality in Heterogeneous Catalysis. *J. Catal.* **2002,** *209*, 275-278.

67. Zhao, Y.; Truhlar, D. G., The M06 Suite of Density Functionals for Main Group Thermochemistry, Thermochemical Kinetics, Noncovalent Interactions, Excited States, and Transition Elements: Two New Functionals and Systematic Testing of Four M06-Class Functionals and 12 Other Functionals. *Theor. Chem. Acc.* **2008,** *120*, 215-241.

68. Zhao, Y.; Truhlar, D. G., Density Functionals with Broad Applicability in Chemistry. *Acc. Chem. Res.* **2008,** *41*, 157-167.

69. Weigend, F.; Ahlrichs, R., Balanced Basis Sets of Split Valence, Triple Zeta Valence and Quadruple Zeta Valence Quality for H to Rn: Design and Assessment of Accuracy. *Phys. Chem. Chem. Phys.* **2005,** *7*, 3297-3305.

70. Wheeler, S. E.; Houk, K. N., Integration Grid Errors for Meta-GGA-Predicted Reaction Energies: Origin of Grid Errors for the M06 Suite of Functionals. *J. Chem. Theory Comput.* **2010,** *6*, 395-404.

71. Marenich, A. V.; Cramer, C. J.; Truhlar, D. G., Universal Solvation Model Based on Solute Electron Density and on a Continuum Model of the Solvent Defined by the Bulk Dielectric Constant and Atomic Surface Tensions. *J. Phys. Chem. B* **2009,** *113*, 6378-6396.

72. Frisch, M. J.; Trucks, G. W.; Schlegel, H. B.; Scuseria, G. E.; Robb, M. A.; Cheeseman, J. R.; Scalmani, G.; Barone, V.; Mennucci, B.; Petersson, G. A.; Nakatsuji, H.; Caricato, M.; Li, X.; Hratchian, H. P.; Izmaylov, A. F.; Bloino, J.; Zheng, G.; Sonnenberg, J. L.; Hada, M.; Ehara, M.; Toyota, K.; Fukuda, R.; Hasegawa, J.; Ishida, M.; Nakajima, T.; Honda, Y.; Kitao, O.; Nakai, H.; Vreven, T.; Montgomery, J. A.; Peralta, J. E.; Ogliaro, F.; Bearpark, M.; Heyd, J. J.; Brothers, E.; Kudin, K. N.; Staroverov, V. N.; Kobayashi, R.; Normand, J.; Raghavachari, K.; Rendell, A.; Burant, J. C.; Iyengar, S. S.; Tomasi, J.; Cossi, M.; Rega, N.; Millam, J. M.; Klene, M.; Knox, J. E.; Cross, J. B.; Bakken, V.; Adamo, C.; Jaramillo, J.; Gomperts, R.; Stratmann, R. E.; Yazyev, O.; Austin, A. J.; Cammi, R.; Pomelli, C.; Ochterski, J. W.; Martin, R. L.; Morokuma, K.; Zakrzewski, V. G.; Voth, G. A.; Salvador, P.; Dannenberg, J. J.; Dapprich, S.; Daniels, A. D.; Farkas; Foresman, J. B.; Ortiz, J. V.; Cioslowski, J.; Fox, D. J., Gaussian 09, Revision D.01. Wallingford CT, 2009.

73. Becke, A. D., Density-Functional Thermochemistry. III. The Role of Exact Exchange. *J. Chem. Phys.* **1993,** *98*, 5648-5652.

74. Lee, C.; Yang, W.; Parr, R. G., Development of the Colle-Salvetti Correlation-Energy Formula into a Functional of the Electron Density. *Phys. Rev. B* **1988,** *37*, 785-789.

75. Steinmann, S. N.; Corminboeuf, C., A System-Dependent Density-Based Dispersion Correction. *J. Chem. Theory Comput.* **2010,** *6*, 1990-2001.

76. Steinmann, S. N.; Corminboeuf, C., A Density Dependent Dispersion Correction. *Chimia* **2011,** *65*, 240-244.

77. Steinmann, S. N.; Corminboeuf, C., A Generalized-Gradient Approximation Exchange Hole Model for Dispersion Coefficients. *J. Chem. Phys.* **2011,** *134*, 044117.

78. Steinmann, S. N.; Corminboeuf, C., Comprehensive Benchmarking of a Density-Dependent Dispersion Correction. *J. Chem. Theory Comput.* **2011,** *7*, 3567-3577.

79. te Velde, G.; Bickelhaupt, F. M.; Baerends, E. J.; Fonseca Guerra, C.; van Gisbergen, S. J. A.; Snijders, J. G.; Ziegler, T., Chemistry with ADF. *J. Comput. Chem.* **2001,** *22*, 931-967.

80. Fonseca Guerra, C.; Snijders, J. G.; te Velde, G.; Baerends, E. J., Towards an order-N DFT method. *Theor. Chem. Acc.* **1998,** *99*, 391-403.

81. Grimme, S., Supramolecular Binding Thermodynamics by Dispersion-Corrected Density Functional Theory. *Chem. Eur. J.* **2012,** *18*, 9955-9964.

82. Mammen, M.; Shakhnovich, E. I.; Deutch, J. M.; Whitesides, G. M., Estimating the Entropic Cost of Self-Assembly of Multiparticle Hydrogen-Bonded Aggregates Based on the Cyanuric Acid·Melamine Lattice. *J. Org. Chem.* **1998,** *63*, 3821-3830.

83. Funes-Ardoiz, I.; Paton, R. S., GoodVibes: version 2.0.3. **2018**, https://doi.org/10.5281/zenodo.1435820.

84. Klamt, A., The COSMO and COSMO-RS solvation models. *WIREs: Comput. Mol. Sci.* **2011,** *1*, 699-709.

85. Heimann, J. E.; Bernskoetter, W. H.; Hazari, N.; Mayer, James M., Acceleration of CO_2 Insertion into Metal Hydrides: Ligand, Lewis Acid, and Solvent Effects on Reaction Kinetics. *Chem. Sci.* **2018,** *9*, 6629-6638.

86. Note that a scan of the potential energy surface revealed no TS for the dissociation of the formate ion from the catalyst. This is because this dissociation process is, overall, thermodynamically unfavorable. For an extensive discussion on the dissociation of ionic compounds in soluation see: Kim, H. J.; Hynes, J. T., *J. Am. Chem. Soc.* **1992**, *114*, 10508-10528.

87. Other Ru pincer catalysts have been shown to facilitate this reaction. For example, see Refs. 27, 28, and 32.

88. Carroll, M. P.; Guiry, P. J., P,N Ligands in Asymmetric Catalysis. *Chem. Soc. Rev.* **2014,** *43*, 819-833.

89. Mitoraj, M. P.; Michalak, A., σ-Donor and π-Acceptor Properties of Phosphorus Ligands: An Insight from the Natural Orbitals for Chemical Valence. *Inorg. Chem.* **2010,** *49*, 578-582.

90. Leis, W.; Mayer, H. A.; Kaska, W. C., Cycloheptatrienyl, Alkyl and Aryl PCP-Pincer Complexes: Ligand Backbone Effects and Metal Reactivity. *Coord. Chem. Rev.* **2008,** *252*, 1787-1797.

TOC Graphic